

A Crystallographic Study of Bright Far-Red Fluorescent Protein mKate Reveals pH-induced *cis-trans* Isomerization of the Chromophore*^[5]

Received for publication, January 23, 2008, and in revised form, June 17, 2008. Published, JBC Papers in Press, August 4, 2008, DOI 10.1074/jbc.M800599200

Sergei Pletnev^{†S1}, Dmitry Shcherbo[¶], Dmitry M. Chudakov[¶], Nadezhda Pletneva[¶], Ekaterina M. Merzlyak^{||}, Alexander Wlodawer^{**}, Zbigniew Dauter[‡], and Vladimir Pletnev[¶]

From the [‡]Macromolecular Crystallography Laboratory, NCI, National Institutes of Health, Argonne, Illinois 60439, the [§]Basic Research Program, SAIC-Frederick Inc., Argonne, Illinois 60439, the [¶]Shemyakin-Ovchinnikov Institute of Bioorganic Chemistry, Russian Academy of Science, 117997 Moscow, Miklukho-Maklaya 16/10, Russia, ^{||}Evrogen JSC, 117997 Moscow, Miklukho-Maklaya 16/10, Russia, and the ^{**}Macromolecular Crystallography Laboratory, NCI-Frederick, National Institutes of Health, Frederick, Maryland 21702

The far-red fluorescent protein mKate (λ_{ex} , 588 nm; λ_{em} , 635 nm; chromophore-forming triad Met⁶³-Tyr⁶⁴-Gly⁶⁵), originating from wild-type red fluorescent progenitor eqFP578 (sea anemone *Entacmaea quadricolor*), is monomeric and characterized by the pronounced pH dependence of fluorescence, relatively high brightness, and high photostability. The protein has been crystallized at a pH ranging from 2 to 9 in three space groups, and four structures have been determined by x-ray crystallography at the resolution of 1.75–2.6 Å. The pH-dependent fluorescence of mKate has been shown to be due to reversible *cis-trans* isomerization of the chromophore phenolic ring. In the non-fluorescent state at pH 2.0, the chromophore of mKate is in the *trans*-isomeric form. The weakly fluorescent state of the protein at pH 4.2 is characterized by a mixture of *trans* and *cis* isomers. The chromophore in a highly fluorescent state at pH 7.0/9.0 adopts the *cis* form. Three key residues, Ser¹⁴³, Leu¹⁷⁴, and Arg¹⁹⁷ residing in the vicinity of the chromophore, have been identified as being primarily responsible for the far-red shift in the spectra. A group of residues consisting of Val⁹³, Arg¹²², Glu¹⁵⁵, Arg¹⁵⁷, Asp¹⁵⁹, His¹⁶⁹, Ile¹⁷¹, Asn¹⁷³, Val¹⁹², Tyr¹⁹⁴, and Val²¹⁶, are most likely responsible for the observed monomeric state of the protein in solution.

Green fluorescent proteins (GFP)² and GFP-like proteins (FP) have become important noninvasive tools for visualization

* This work was supported, in whole or in part, by the National Institutes of Health Intramural Research Program of the Center for Cancer Research, NCI, and with Federal funds from NCI Contract No. NO1-CO-12400. This work was also supported by the Russian Foundation for Basic Research (Grants 07-04-00054 and 07-04-12189), Russian Federal Agency for Science and Innovations (Grant 02.513.12.3013). The costs of publication of this article were defrayed in part by the payment of page charges. This article must therefore be hereby marked "advertisement" in accordance with 18 U.S.C. Section 1734 solely to indicate this fact.

The atomic coordinates and structure factors (codes 3BX9, 3BXA, and 3BXB) have been deposited in the Protein Data Bank, Research Collaboratory for Structural Bioinformatics, Rutgers University, New Brunswick, NJ (<http://www.rcsb.org/>).

^[5] The on-line version of this article (available at <http://www.jbc.org/>) contains supplemental "Experimental Procedures" and Fig. S1.

[†] To whom correspondence should be addressed: SAIC-Frederick Inc., Basic Research Program, Argonne, IL 60439. E-mail: svp@ncifcrf.gov.

² The abbreviations used are: GFP, green fluorescent protein; PEG, polyethylene glycol; PDB, Protein Data Bank; R.M.S.D., root mean-squared deviation.

and monitoring of the internal processes within cells or whole organisms, such as gene expression, monitoring the cellular pH, ion concentration, embryogenesis, inflammatory processes, tracking protein trafficking, the migration of parasites within a host, *etc* (1–13). Fluorescent proteins can be used to visualize many types of cancer processes, including primary tumor growth, tumor cell motility and invasion, metastatic seeding and colonization, angiogenesis, and interactions between the tumor and its host microenvironment (14–16). FPs might be very useful in real-time testing of the efficacy of cancer drugs in animal models of human cancer.

The extensive spectral diversity of fluorescent proteins arises mostly from variations in the chemical structure of the mature chromophore and in the stereochemistry of its adjacent environment. The FP chromophore forms autocatalytically *in vivo* and *in vitro* from three residues, Xxx-Tyr-Gly, without need for any cofactors or enzymes, except for molecular oxygen (17). In most cases, the post-translational modification results in a blue/green emitting state, characterized by formation of an imidazolinone heterocycle with a *p*-hydroxybenzylidene substituent. Often, the reaction chain propagates further with formation of an additional *N*-acylimine double bond, which extends the conjugation of the chromophore π electronic system and results in a bathochromic shift in spectra (18–22).

Proteins that emit red, and especially far-red light, are of particular interest (13). The longer wavelength light extends the range of fluorescence resonance energy transfer (FRET)-based applications and causes fewer damaging events to proteins and DNA because of its lower energy. The most favorable "optical window" for the visualization in living tissues is ~650–1100 nm (23). Light with wavelength longer than 1100 nm is absorbed by water. Detection of fluorescence from proteins with emission peaks much shorter than 650 nm encounters the problem of interfering cellular autofluorescence. At present the brightest red fluorescent proteins have emission maxima too far from the preferred "optical window." Besides, their excitation maxima are located in a range 550–560 nm, where living tissues are almost opaque and fluorescence of these proteins cannot be effectively excited (see Table 1 in Ref. 13). Recently, far-red fluorescent variants, HcRed, mPlum, and AQ143, reaching the 650 nm barrier, have been developed (24–26).

However, these proteins are characterized by low brightness, strongly limiting their practical application.

A majority of the wild-type GFP-like proteins form tetramers, complicating their practical use. To be the most useful tools for practical applications, the designed biomarkers should preferably exist in a monomeric form, emit in the far-red fluorescent spectral range, have high brightness, be photostable, and exhibit a high rate of chromophore maturation. It has always been difficult to develop variants meeting all of these criteria simultaneously. Recently, however, the bright far-red dimeric variant Katushka and its monomeric version mKate, both characterized by a chromophore-forming sequence, Met⁶³-Tyr⁶⁴-Gly⁶⁵, have been successfully designed (13). Both proteins, characterized by similar spectral properties (λ_{ex} , 588 nm; λ_{em} , 635 nm), are derived from wild-type red fluorescent progenitor eqFP578 (*Entacmaea quadricolor*), the latter having spectral maxima λ_{ex} , 552 nm; λ_{em} , 578 nm. Both Katushka and mKate are significantly brighter than the spectrally close HcRed or mPlum (24, 25) and display fast maturation, as well as high pH- and photo-stability. The fluorescence of Katushka and mKate is pH-dependent, showing maximum emission at pH \sim 8, which gradually diminishes to zero at pH \sim 4. Compared with other far-red FPs, Katushka exhibits evident superiority for visualization in living tissues. The monomeric mKate is an excellent fluorescent label for monitoring fused proteins in whole organisms, multicolor labeling, and FRET applications.

We present here the results of crystallographic studies of three-dimensional structures of the far-red variant mKate in different fluorescent states, corresponding to pH 2.0, 4.2, and 7.0. These structures were solved at resolution ranging from 1.75 to 2.6 Å. We have analyzed in detail the stereochemical features in the chromophore area that are responsible for the outstanding spectral characteristics of the protein and its relatively high pH dependence of fluorescence, as well as the nature of surface residues responsible for the predominantly monomeric state of the protein.

EXPERIMENTAL PROCEDURES

The details of cloning, purification, and characterization of the studied proteins are presented in supplemental "Experimental Procedures."

Crystallization, Structure Solution, and Crystallographic Refinement—Crystals have been obtained by the hanging drop vapor diffusion method in four different conditions. The mKate_pH2.0 crystals have appeared from 20% w/v PEG 3350, 0.2 M ammonium citrate tribasic, 0.4 M citric acid, pH 2.0, initial protein concentration 12 mg/ml. The mKate_pH4.2 was crystallized from 17.5% (w/v) PEG 3350, 0.07 M citric acid, pH 4.2, initial protein concentration 15 mg/ml. Crystals of mKate_pH7.0 and mKate_pH9.0 were grown from 20% w/v PEG6000, 1 M LiCl, 0.1 M HEPES pH 7.0, and 20% w/v PEG6000, 1 M LiCl, 0.1 M Bicine pH 9.0, respectively. Initial protein concentration for both conditions was 18 mg/ml.

X-ray diffraction data were collected from single crystals flash-cooled in a 100 K nitrogen stream. Prior to cooling, the crystals were transferred to a cryo-protecting solution containing 20% glycerol and 80% reservoir solution. Data were collected with a MAR300 CCD detector at the SER-CAT beamline

22ID (Advanced Photon Source, Argonne National Laboratory, Argonne, IL) and were processed with *HKL2000* (27).

Crystal structure of mKate at pH 4.2 was solved by the molecular replacement method with *MOLREP* (28, 29), using the coordinates of the eqFP611 monomer without the chromophore (71% sequence identity, PDB ID: 1UIS; (19)). The refined coordinates of mKate at pH 4.2 were used to solve the other mKate structures at pH 2.0, 7.0, and 9.0. Structure refinement was performed with *REFMAC5* (30) and *PHENIX* (31), alternating with manual revision of the model using *COOT* (32). Water molecules were located with *ARP/wARP* (33). Non-crystallographic symmetry restraints were applied in refinement of mKate_pH7.0 and mKate_pH9.0 structures with eight subunits in asymmetric unit. The occupancy of each chromophore state was set to reach the best possible agreement between the model and difference electron density map. Crystallographic data and refinement statistics are presented in Table 1. Although the values of R_{merge} were relatively high in the outermost shells of all data sets, the corresponding values of $I/\sigma(I)$ indicated that these data were still significant.

Structure validation was performed with *PROCHECK* (34). The coordinates and structure factors were deposited in the Protein Data Bank under accession codes 3BX9 (mKate_pH2.0), 3BXA (mKate_pH4.2), 3BXB (mKate_pH7.0). The structure at pH 9.0 (accession code 3BXC) was found almost identical to the structure at pH 7.0 and was skipped from discussion.

RESULTS AND DISCUSSION

Electron Density Interpretation—The asymmetric unit in mKate_pH2.0 and mKate_pH4.2 crystals contains one dimer. Crystallographic symmetry operations transform the dimers to the corresponding tetramers. The asymmetric unit in mKate_pH7.0 possesses two tetramers. The electron density for all structures allowed unambiguous fitting of residues 2/3/4–228 for all monomers in the asymmetric unit. No density was observed for the N-terminal His tag fragment introduced into the expressed construct and used for protein purification. The relatively high resolution \sim 1.8 Å of the low pH structures enabled us to detect alternative stable conformations for a number of side chains. We located between 259 and 351 hydrogen-bonded water molecules in the asymmetric unit of each crystal. Several citric acid and glycerol molecules (the components of the crystallization and cryoprotectant solutions) were located in the mKate_pH2.0 and mKate_pH4.2 structures.

Monomer Structure—The principal structural fold of the mKate is an 11-stranded β -barrel, closed from both sides by loop caps, with a chromophore (matured from the sequence Met⁶³-Tyr⁶⁴-Gly⁶⁵) embedded in the middle of an internal α -helix that is wound along the β -barrel axis. The C-terminal tail 222–228 has irregular conformation and goes away from the β -barrel body. The R.M.S.D. values from pairwise superposition of the mKate monomer structures corresponding to different pH are within the range of 0.32–0.41 Å for all equivalent C $^{\alpha}$ atoms, indicating a very similar fold of the monomers. Two *cis* peptide bonds preceding Pro⁵⁰ and Pro⁸⁵ in the loop area have been detected. Similarly to TurboGFP and the FPs from *Zoanthus* (22, 35), the β -barrel frame of mKate shows the presence of a pore, formed by the backbone of Trp¹⁴⁰, Glu¹⁴¹,

The Structure of Bright Far-Red Fluorescent Protein mKate

TABLE 1
Crystallographic data and refinement statistics

Protein	mKate pH 2.0 (PDB_ID: 3BX9)	mKate pH 4.2 (PDB_ID: 3BXA)	mKate pH 7.0 (PDB_ID: 3BXB)
Crystallographic data			
Space group	P6 ₅ 22	I4	P2 ₁
Cell dimensions (Å, °)	<i>a</i> , <i>b</i> = 67.9, <i>c</i> = 413.0	<i>a</i> , <i>b</i> = 98.2, <i>c</i> = 106.5	<i>a</i> = 74.2, <i>b</i> = 105.0, <i>c</i> = 123.0 <i>β</i> = 105.8
Z/(Z')	24 (2)	16 (2)	16 (8)
Estimated solvent content (%)	51	47	41
Temperature (K)	100	100	100
Wavelength (Å)	1.00	1.00	1.00
Resolution range (Å)	30.0–1.80 (1.86–1.80) ^a	30.0–1.75 (1.81–1.75) ^a	30.0–2.60 (2.69–2.60) ^a
Total reflections measured	762,295	387,816	210,733
Unique reflections observed (F > 0)	53,955	50,567	55,386
Redundancy	14.1 (14.4) ^a	7.7 (7.6) ^a	3.8 (3.4) ^a
I/σ(I)	46.1 (5.6) ^a	43.9 (3.7) ^a	11.6 (2.1) ^a
R _{merge}	0.061 (0.556) ^a	0.041 (0.522) ^a	0.122 (0.506) ^a
Completeness	99.9 (99.7) ^a	99.6 (99.1) ^a	99.9 (99.4) ^a
Refinement statistics			
Non-H atoms in model			
Protein	3,586 [2 x (2–228) res]	3,574 [2 x (3–228) res]	14,224 [8 x (4–228) res]
Water	259	302	351
Citrate	78 (6 mol)	13 (1mol)	
Glycerol	12 (2 mol)		
R _{work}	0.204 (97.9%) ^b	0.180 (97.9%) ^b	0.170 (94.8%) ^b
R _{free}	0.247 (2.1%) ^b	0.232 (2.1%) ^b	0.263 (5.2%) ^b
Mean B factor/(R.M.S.D.) (Å²)			
Protein atoms			
Main chain	25.5 (0.8)	26.4 (0.7)	39.1 (0.5)
Side chain	28.3 (1.8)	28.9 (1.8)	39.4 (1.0)
Chromophore	23.4 (2.8)	23.4 (2.2)	37.1 (1.5)
Ramachandran statistics (%) (for non-Gly/Pro residues)			
Most favorable/additional allowed	91.1/8.9	91.3/8.7	87.4/12.6
Generously allowed/disallowed regions	0.0/0.0	0.0/0.0	0.0/0.0

^a Values for the data in the highest resolution shell.

^b Percent of the data reserved for working and free sets.

Ala1⁴², Arg¹⁹⁷, Arg¹⁹⁸, and Leu¹⁹⁹, leading to the hydroxyphenyl moiety of the chromophore. A chain of hydrogen-bonded water molecules, going through the pore from the outside, could be identified in the mKate_pH2.0 and mKate_pH4.2 structures. Evdokimov *et al.* (35) suggested that this pore is essential for chromophore maturation, providing access for molecular oxygen.

Monomer Association—According to gel filtration data, mKate exists in solution in the monomeric state at concentration as high as 10 mg/ml (13). However, in the crystalline state, which corresponds to a much higher protein concentration, mKate adopts at all pH values tetrameric arrangement with 222 symmetry, typically seen in GFP-like proteins. The interacting surfaces of the subunits create two types of interfaces. Interface IF1 is located between two antiparallel monomers that form an “antiparallel” dimer (A-dimer), whereas the IF2 interface is found between two monomers belonging to adjacent A-dimers. Those monomers positioned at ~75° with respect to each other form a “crossed” dimer (C-dimer) (Table 2). The irregular C-terminal tail, consisting of residues 222–228, goes away from the β-barrel and sticks to cylindrical surface of the interacting counterpart, contributing to the IF2-contacting surface.

The tetrameric assemblies of mKate in the crystal forms grown at different pH have similar topology but exhibit significant packing differences. The pairwise three-dimensional superposition of the tetramers for all equivalent C^α atoms gives the following values of R.M.S.D. for corresponding pairs: mKate_pH7.0 and mKate_pH2.0; 1.85 Å, mKate_pH4.2 and mKate_pH2.0; 2.61 Å, mKate_pH4.2 and mKate_pH7.0; 4.30 Å.

TABLE 2
Characteristics of the tetramer interfaces

mKate_pH2.0		mKate_pH4.2		mKate_pH7.0	
Intratetramer contact area (Å ²) ^a					
IF1 690	IF2 1500	IF1 300	IF2 1490	IF1 930	IF2 1490
Interface-stabilizing H-bonds/salt-bridges (within 3.3 Å)					
4	17	10	23	13	25
Angle between β-barrel axes in an A/C-dimer ^b (°)					
A 31	C 75	A 41	C 74	A 23	C 72

^a Half of the buried surface area at the dimer interface corresponding to a radius of the probe solvent molecule 1.4 Å.

^b The axis goes through C^α atoms of residues 60 and 67 of the central α-helix.

The IF1 interface within the A-dimer is noticeably weaker, compared with the IF2 interface within the C-dimer. In the structures reported here, IF1 exhibits significant variation in its contact area, the number and composition of stabilizing interactions, and the angle between the antiparallel β-barrel axes (Table 2). In all crystal forms, the IF2 interfaces are more extensive and more uniform than the IF1 interfaces.

Although the monomeric mKate and the dimeric Katushka have similar spectral characteristics (λ_{ex}, 588 nm, λ_{em}, 635 nm; (13)), a comparison of their primary structures shows 18 differences (Fig. 1). Three of them, corresponding to positions 93, 122, and 155 are situated at the interface IF1, whereas eight differences at positions 157, 159, 169, 171, 173, 192, 194, and 216 are found at the IF2 interface. At least some of these differences must be responsible for the observed variation of the oligomeric states of these proteins in solu-

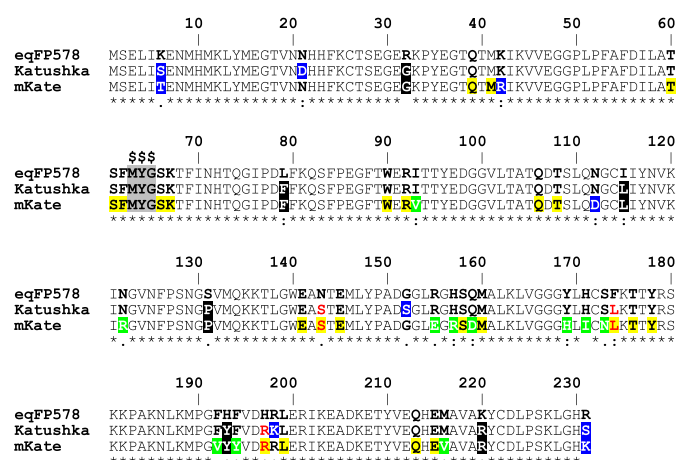


FIGURE 1. Sequence alignment of the wild-type eqFP578 and its mutant far-red variants, Katushka and mKate. Residue positions in three-dimensional structure: \$, chromophore forming residues. *Black* and *red* font (highlighted in *yellow*), chromophore nearest environment (see Figs. 4 and 5). *Red*, chromophore environment; apparently responsible for the far-red shift. *White* font (highlighted in *black*), β -barrel caps area; presumably silent mutations or covariant with those in *red*. *White* font (highlighted in *green*), crystal intratetramer interfaces; apparently responsible for monomerization in solution. *White* font (highlighted in *blue*), presumably silent mutations in random mutagenesis process.

tion. These 11 interface positions (highlighted in *green* for mKate in Fig. 1) are occupied by identical amino acids in Katushka and its wild-type progenitor eqFP578, both of which form dimers in solution (13, 36).

pH-induced cis-trans Isomerization of the Chromophore—The spectral properties of the far-red fluorescent protein mKate have been comprehensively investigated by Shcherbo *et al.* (13). The protein exhibits maximum emission at pH \sim 8, gradually disappearing at pH \sim 4 (Fig. 2*a*). In mKate the post-translational modification of the chromophore-forming sequence Met⁶³-Tyr⁶⁴-Gly⁶⁵ results in a conventional GFP two ring-conjugated core consisting of a five-membered imidazolinone heterocycle with a *p*-hydroxybenzylidene substituent. Similar to other red and far-red fluorescent proteins (18–20, 37, 38), the first chromophore residue Met⁶³ in mKate is characterized by formation of an *N*-acylimine partially double bond, N=C α , the *sp*² hybridization of the corresponding C α atom, and the *cis* configuration of the preceding peptide bond. An additional *N*-acylimine bond apparently extends the chromophore-conjugated π electronic system, resulting in a bathochromic shift in spectra.

The unique feature of mKate, revealed by this study, is the observed pH-induced *cis-trans* isomerization of the chromophore Tyr⁶⁴ phenolic ring with respect to the C α -N bond. The predominant *trans* conformation of the phenolic ring (Fig. 3*A*) was detected in the mKate_pH2.0 crystal structure that corresponds to the non-fluorescent (dark) state (Fig. 2). The difference electron density indicates the presence of \sim 10% of the *cis* isomer. In contrast, the highly fluorescent (bright) state of the mKate_pH7.0 structure is characterized by a mostly *cis* conformation of the phenolic ring, with \sim 10% contamination by *trans* isomer in four out of eight independent subunits (Fig. 3*C*). The structure of mKate_pH4.2, exhibiting a low level of fluorescence, shows the presence of both the *trans* and *cis* iso-

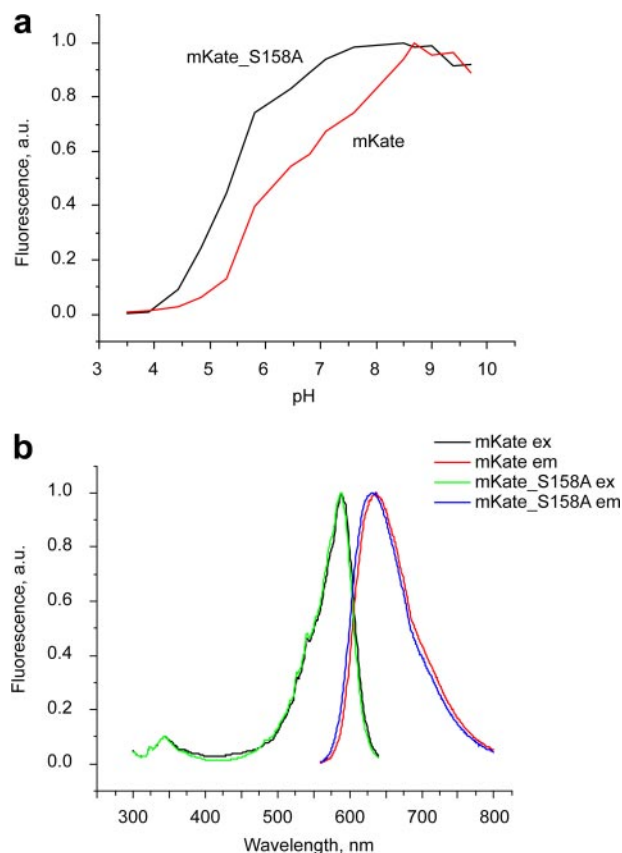


FIGURE 2. mKate and rationally designed structure-based variant mKate_S158A. *a*, pH dependence of the fluorescence; *b*, fluorescence spectra.

mers in a ratio \sim 60% to \sim 40% in subunit *A* (Fig. 3*B*) and \sim 80% to \sim 20% in subunit *B*.

Both the *trans* and *cis* forms of the chromophore, representing the dark and the bright states, respectively, exhibit noticeable distortion from coplanarity of the imidazolinone and phenolic rings. In two subunits of the mKate_pH2.0 crystal structure with the *trans* chromophore, the values of χ^1 and χ^2 torsion angles around the C α =C β and C β -C γ bonds of the tyrosine are relatively low, \sim 173 $^\circ$ (7 $^\circ$ deviation from the ideal planar form) and \sim 15 $^\circ$ respectively. In eight subunits of the mKate_pH7.0 structure with a *cis* chromophore, these angles are \sim 1 $^\circ$ and $25 \pm 5^\circ$, respectively. In FPs, both chromophore rings generally are more coplanar in the *cis* than in the *trans* arrangement (Table 3*B* in Ref. 39). Non-coplanar ring arrangement was mostly associated with the non-fluorescent state. However, the observed coplanarity of the *trans* chromophore in eqFP611 (19) and the non-coplanarity of the *cis* chromophore in the fluorescent variant of Rtms5 (40) show that this is not always the case. In mKate, the non-coplanar *cis* chromophore (with a relatively large value of χ^2), exhibits high fluorescence. We suggest that the energy difference between nonplanar and planar chromophore conformations is small and could be overcome by light excitation. In other words, the nonplanar conformation of the *cis* chromophore observed in the crystals presumably corresponds to the resting state, which at small energy expense may be transformed to planar conformation in the excited fluorescent state. The bond angle C α -C β -C γ of Tyr⁶⁴

The Structure of Bright Far-Red Fluorescent Protein mKate

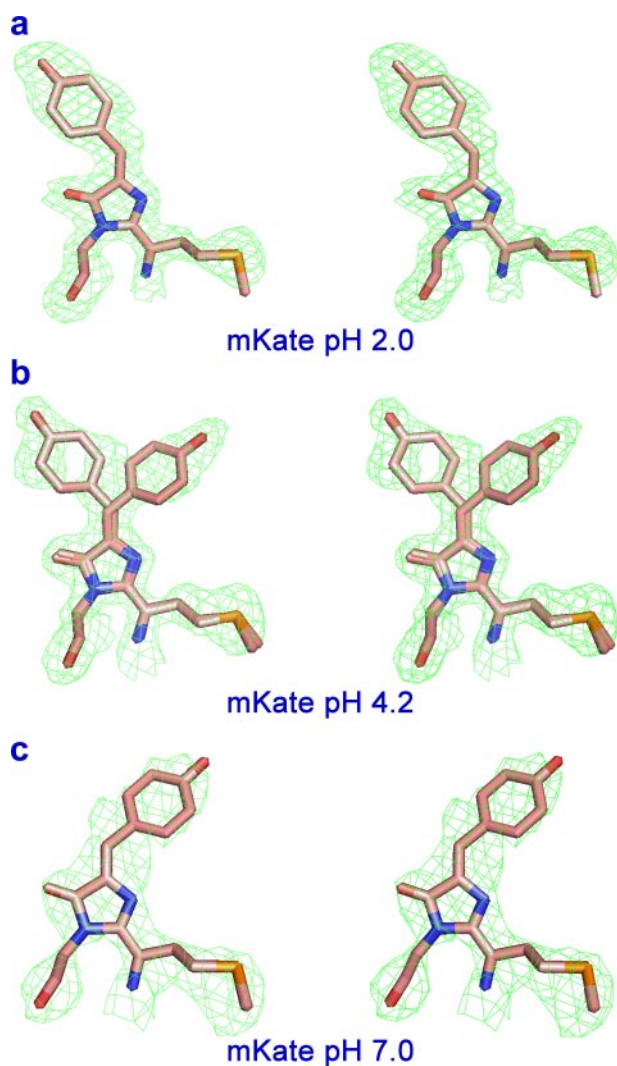


FIGURE 3. A stereoview of the chromophores in a difference Fo-Fc electron density (cutoff $\rho = 3.0 \sigma$). This was calculated with the phases omitting the contribution of the chromophore in the mKate crystal structures at pH 2.0 (a), pH 4.2 (subunit A) (b), pH 7.0 (c). This figure was produced with Pymol (44).

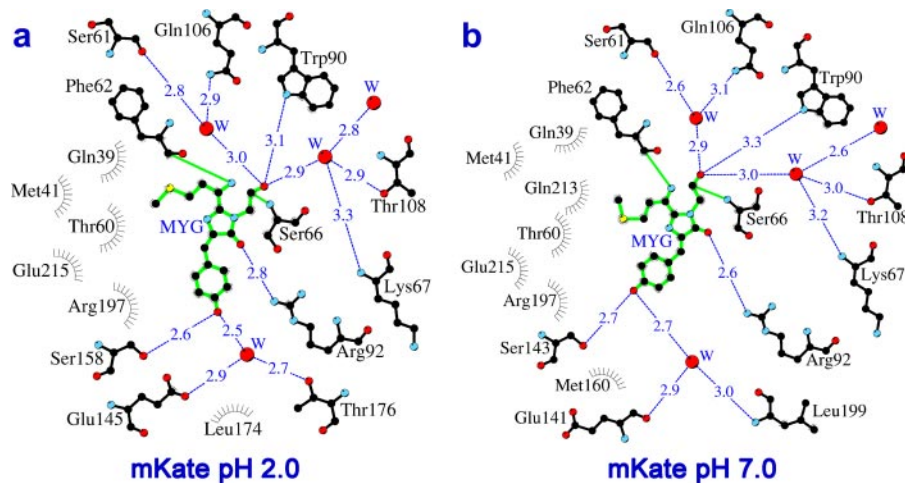


FIGURE 4. A schematic diagram illustrating the environment of the *trans* chromophore in the mKate_pH2.0 structure (a) and the *cis* chromophore in the mKate_pH7.0 structure (b). Hydrogen bonds ($\leq 3.3 \text{ \AA}$) are shown as blue dashed lines, waters (W) as red spheres, and van der Waals contacts ($\leq 3.9 \text{ \AA}$) as black "eyelashes." This figure was produced with LIGPLOT/HBPLUS (45, 46).

observed in the *trans* mKate chromophore is 5° larger than that in the *cis* chromophore ($\sim 135^\circ$ versus $\sim 130^\circ$). This difference, as well as the deviation from planarity of the *trans* chromophore, apparently arises from the steric repulsion between C^{δ} and carbonyl O atoms of Tyr⁶⁴.

Different geometric restraint schemes were tested to determine the optimal geometry of the group (63) $C^{\alpha}=N-C(O)-C^{\alpha}$ (62) bridging the C^{α} atoms of the first chromophore residue Met⁶³ and the preceding Phe⁶². Similar to HcRed (38), it exhibits, at optimal fit to electron density, considerable deviation from planarity with ω torsion angle around the quasi-peptide N-C(O) bond in a range $20-35^\circ$. Moreover, similarly to other red and far-red fluorescent proteins (18, 19, 22, 38), the C(O)-N-C $^{\alpha}$ bond angle of the linkage in both chromophore isomers is strongly linearized, in the range of $140-160^\circ$. The nature of such unusual geometry of the linkage is not clear. It may be assumed that steric tension in the central α -helix that, according to a hypothesis of Barondeau *et al.* (17), drives chromophore formation, might leave in the mature structure some remnant strain, partially responsible for the observed effect. The equilibrium strain relaxation is presumably achieved at the expense of the compromised distortion of the linkage preceding the chromophore.

The chromophore in the *trans* and *cis* conformations makes three direct H-bonds ($\leq 3.3 \text{ \AA}$) with the side chains of the protein, three H-bonds with water molecules (each water molecule mediates H-bonding with two residues), and the respective 106 and 93 van der Waals contacts ($\leq 3.9 \text{ \AA}$) (Fig. 4). Two of the three direct H-bonds are formed by the carbonyls of Tyr⁶⁴ and Gly⁶⁵ of the chromophore, interacting with the side chains of Arg⁹² and Trp⁹⁰, respectively. The third H-bond is formed between the hydroxyl of Tyr⁶⁴ and the side chains of either Ser¹⁵⁸ or Ser¹⁴³ in the *trans* or *cis* conformational states, respectively.

The consensus part of the chromophore nearest shell in the mKate_pH2.0 and mKate_pH7.0 structures is composed of 17 residues, most of which are involved in an extensive H-bond network formed by the side chain and backbone interactions (Fig. 5). Among them are the catalytic residues, Glu²¹⁵, Arg⁹², and Thr⁶⁰. Five proximal waters (presumed reaction products of the maturation process) are actively involved in forming the network-mediating residue interactions. The hydrogen-bonded network interacts with the chromophore and is apparently functionally important, creating a potential proton wire in the maturation process.

Surprisingly, the positions of the imidazolinone rings, as well as the three-dimensional arrangements of the side chains in the chromophore environment, are practically identical in mKate_pH2.0 and mKate_pH7.0. In both the *trans* and *cis* states the phenolic ring almost

TABLE 3
Spectral characteristics of mKate and mKate_S158A

Protein	Excitation maximum	Emission maximum	QY	EC, at ex max	Relative brightness ^a	pK _a
				<i>M</i> ⁻¹ <i>cm</i> ⁻¹		
mKate	588	635	0.33	45,000	0.45	6.2
mKate_S158A	588	633	0.40	70,000	0.85	5.3

^a Brightness is calculated as a product of the molar extinction coefficient and the fluorescence quantum yield and is given by comparison to the brightness of EGFP.

power at low pH. The mKate_S158A variant was prepared, and we compared its spectral and biochemical characteristics with those of mKate (Fig. 2 and Table 3). mKate_S158A is a bright fluorescent protein with λ_{ex} , 588 nm; λ_{em} , 633 nm; *i.e.* emission spectra is slightly blue-shifted, compared with mKate (Fig. 2*b*). As expected, this variant is characterized by substantially higher pH stability (Fig. 2*a*), with pK_a = 5.3, compared with 6.2 of mKate. The mKate_S158A is characterized by an essentially higher molar extinction and also by a higher fluorescence quantum yield, resulting in almost 2-fold brighter fluorescence, as well as by a higher rate of chromophore maturation. In contrast to mKate, at physiological pH 7.0–7.5 it demonstrates no kindling effect upon irradiation by excitation light, in agreement with the *trans-cis* isomerization hypothesis of kindling effect (42, 43). At this pH, characterized by relatively low level of cumulative protonation, the equilibrium state of the mKate chromophore has approximately ~10% fraction of the *trans*-form. Photoactivation of mKate by light irradiation causes switching of the remaining dark *trans*-form to the fluorescent *cis*-form, resulting in gradual increase of the intensity at fluorescence maximum by an additional ~10%. Reverse transformation was found to be less favorable. At physiological pH the chromophore of mKate_S158A is, presumably, in ~100% *cis*-form, thus irradiation does not cause the kindling effect. In addition, the photostability of mKate_S158A is comparable to that of the highly photostable mKate, making it an excellent fluorescent tag for labeling of fusion proteins in the far-red part of the visible spectrum.

Acknowledgments—We acknowledge the use of beamline 22-ID of the Southeast Regional Collaborative Access Team (SER-CAT), located at the Advanced Photon Source, Argonne National Laboratory. Use of the APS was supported by the United States Department of Energy, Office of Science, Office of Basic Energy Sciences, under Contract No. W-31-109-Eng-38. The content of this publication does not necessarily reflect the views or policies of the Department of Health and Human Services, nor does the mention of trade names, commercial products or organizations imply endorsement by the U.S. Government.

REFERENCES

- (1998) *Green Fluorescent Protein: Properties, Applications, and Protocols*, pp. 120–171, Wiley-Liss, New York
- Tsien, R. Y. (1998) *Annu. Rev. Biochem.* **67**, 509–544
- Haugwitz, M., Dery, O., Turpin, P., and Fang, Y. (2003) *Genet. Eng. News* **23**, 36–39
- Zubova, N. N., and Savitsky, A. P. (2005) *Uspekhi Biol. Khim. (Rus)* **45**, 1–66
- Verkhusha, V. V., and Lukyanov, K. A. (2004) *Nat. Biotechnol.* **22**, 289–296
- Chudakov, D. M., Lukyanov, S., and Lukyanov, K. A. (2005) *Trends Biotechnol.* **23**, 605–613

- Tallini, Y. N., Ohkura, M., Choi, B. R., Ji, G., Imoto, K., Doran, R., Lee, J., Plan, P., Wilson, J., Xin, H. B., Sanbe, A., Gulick, J., Mathai, J., Robbins, J., Salama, G., Nakai, J., and Kotlikoff, M. I. (2006) *Proc. Natl. Acad. Sci. U. S. A.* **103**, 4753–4758
- Remington, S. J. (2006) *Curr. Opin. Struct. Biol.* **16**, 714–721
- Passamaneck, Y. J., Di, G. A., Papaioannou, V. E., and Hadjantonakis, A. K. (2006) *Microsc. Res. Tech.* **69**, 160–167
- Stewart, C. N., Jr. (2006) *Trends Biotechnol.* **24**, 155–162
- Seitz, G., Warmann, S. W., Fuchs, J., Mau-Holzmann, U. A., Ruck, P., Heitmann, H., Hoffman, R. M., Mahrt, J., Muller, G. A., and Wessels, J. T. (2006) *J. Pediatr. Surg.* **41**, 1369–1376
- Wacker, S. A., Oswald, F., Wiedenmann, J., and Knochel, W. (2007) *Dev. Dyn.* **236**, 473–480
- Shcherbo, D., Merzlyak, E. M., Chepurnykh, T. V., Fradkov, A. F., Ermakova, G. V., Solovieva, E. A., Lukyanov, K. A., Bogdanova, E. A., Zarskiy, A. G., Lukyanov, S., and Chudakov, D. M. (2007) *Nat. Methods* **4**, 741–746
- Hoffman, R. M. (2005) *J. Biomed. Opt.* **10**, 41202
- Hoffman, R. M. (2005) *Curr. Top. Dev. Biol.* **70**, 121–144
- Hoffman, R. M. (2005) *Nat. Rev. Cancer* **5**, 796–806
- Barondeau, D. P., Putnam, C. D., Kassmann, C. J., Tainer, J. A., and Getzoff, E. D. (2003) *Proc. Natl. Acad. Sci. U. S. A.* **100**, 12111–12116
- Yarbrough, D., Wachter, R. M., Kallio, K., Matz, M. V., and Remington, S. J. (2001) *Proc. Natl. Acad. Sci. U. S. A.* **98**, 462–467
- Petersen, J., Wilmann, P. G., Beddoe, T., Oakley, A. J., Devenish, R. J., Prescott, M., and Rossjohn, J. (2003) *J. Biol. Chem.* **278**, 44626–44631
- Tubbs, J. L., Tainer, J. A., and Getzoff, E. D. (2005) *Biochemistry* **44**, 9833–9840
- Pakhomov, A. A., Pletneva, N. V., Balashova, T. A., and Martynov, V. I. (2006) *Biochemistry* **45**, 7256–7264
- Pletneva, N., Pletnev, V., Tikhonova, T., Pakhomov, A. A., Popov, V., Martynov, V. I., Wlodawer, A., Dauter, Z., and Pletnev, S. (2007) *Acta Crystallogr. Sect. D Biol. Crystallogr.* **63**, 1082–1093
- Konig, K. (2000) *J. Microsc.* **200**, 83–104
- Gurskaya, N. G., Fradkov, A. F., Tersikh, A., Matz, M. V., Labas, Y. A., Martynov, V. I., Yanushevich, Y. G., Lukyanov, K. A., and Lukyanov, S. A. (2001) *FEBS Lett.* **507**, 16–20
- Wang, L., Jackson, W. C., Steinbach, P. A., and Tsien, R. Y. (2004) *Proc. Natl. Acad. Sci. U. S. A.* **101**, 16745–16749
- Shkrob, M. A., Yanushevich, Y. G., Chudakov, D. M., Gurskaya, N. G., Labas, Y. A., Poponov, S. Y., Mudrik, N. N., Lukyanov, S., and Lukyanov, K. A. (2005) *Biochem. J.* **392**, 649–654
- Otwinowski, Z., and Minor, W. (1997) *Methods Enzymol.* **276**, 307–326
- Collaborative Computational Project No. 4 (1994) *Acta Crystallogr. Sect. D Biol. Crystallogr.* **50**, 760–763
- Vagin, A., and Teplyakov, A. (1997) *J. Appl. Crystallogr.* **30**, 1022–1025
- Murshudov, G. N., Vagin, A. A., and Dodson, E. J. (1997) *Acta Crystallogr. Sect. D Biol. Crystallogr.* **53**, 240–255
- Adams, P. D., Grosse-Kunstleve, R. W., Hung, L. W., Ioerger, T. R., McCoy, A. J., Moriarty, N. W., Read, R. J., Sacchettini, J. C., Sauter, N. K., and Terwilliger, T. C. (2002) *Acta Crystallogr. Sect. D Biol. Crystallogr.* **58**, 1948–1954
- Emsley, P., and Cowtan, K. (2004) *Acta Crystallogr. Sect. D Biol. Crystallogr.* **60**, 2126–2132
- Perrakis, A., Sixma, T. K., Wilson, K. S., and Lamzin, V. S. (1997) *Acta Crystallogr. Sect. D Biol. Crystallogr.* **53**, 448–455
- Laskowski, R. A., MacArthur, M. W., Moss, D. S., and Thornton, J. M. (1993) *J. Appl. Crystallogr.* **26**, 283–291
- Evdokimov, A. G., Pokross, M. E., Egorov, N. S., Zarskiy, A. G., Yampolsky, I. V., Merzlyak, E. M., Shkorporov, A. N., Sander, I., Lukyanov, K. A., and Chudakov, D. M. (2006) *EMBO Rep.* **7**, 1006–1012
- Merzlyak, E. M., Goedhart, J., Shcherbo, D., Bulina, M. E., Shcheglov, A. S., Fradkov, A. F., Gaintzeva, A., Lukyanov, K. A., Lukyanov, S., Gadella, T. W., and Chudakov, D. M. (2007) *Nat. Methods* **4**, 555–557
- Wall, M. A., Socolich, M., and Ranganathan, R. (2000) *Nat. Struct. Biol.* **7**, 1133–1138
- Wilmann, P. G., Petersen, J., Pettikiriarachchi, A., Buckle, A. M., Smith, S. C., Olsen, S., Perugini, M. A., Devenish, R. J., Prescott, M., and Rossjohn, J. (2005) *J. Mol. Biol.* **349**, 223–237

39. Quillin, M. L., Anstrom, D. M., Shu, X., O'Leary, S., Kallio, K., Chudakov, D. M., and Remington, S. J. (2005) *Biochemistry* **44**, 5774–5787
40. Prescott, M., Ling, M., Beddoe, T., Oakley, A. J., Dove, S., Hoegh-Guldberg, O., Devenish, R. J., and Rossjohn, J. (2003) *Structure* **11**, 275–284
41. He, X., Bell, A. F., and Tonge, P. J. (2003) *FEBS Lett.* **549**, 35–38
42. Chudakov, D. M., Feofanov, A. V., Mudrik, N. N., Lukyanov, S., and Lukyanov, K. A. (2003) *J. Biol. Chem.* **278**, 7215–7219
43. Andresen, M., Wahl, M. C., Stiel, A. C., Gräter, F., Schafer, L. V., Trowitzsch, S., Weber, G., Eggeling, C., Grubmüller, H., Hell, S. W., and Jakobs, S. (2005) *Proc. Natl. Acad. Sci. U. S. A.* **102**, 13070–13074
44. DeLano, W. L. (2002) The PyMOL Molecular Graphics System
45. Wallace, A. C., Laskowski, R. A., and Thornton, J. M. (1995) *Protein Eng.* **8**, 127–134
46. McDonald, I. K., and Thornton, J. M. (1994) *J. Mol. Biol.* **238**, 777–793
47. Evans, S. V. (1993) *J. Mol. Graph.* **11**, 134–138
48. Ho, S. N., Hunt, H. D., Horton, R. M., Pullen, J. K., and Pease, L. R. (1989) *Gene* **77**, 51–59